Centrum Wiskunde & Informatica

On Challenges in Quantitative Photoacoustic Tomography and Ultrasound Computed Tomography

Felix Lucka, joint struggle with Lu An, Simon Arridge, Paul Beard, Ben Cox, Robert Ellwood, Martina Bargeman Fonseca, Ashkan Javaherian, Emma Malone & Brad Treeby.

Mathematical and Numerical Approaches for Multi-Wave Inverse Problems
Marseille
2 April 2019

H2020 Project: Novel Photoacoustic Mammography Scanner

New diagnostic information from optical and acoustic properties

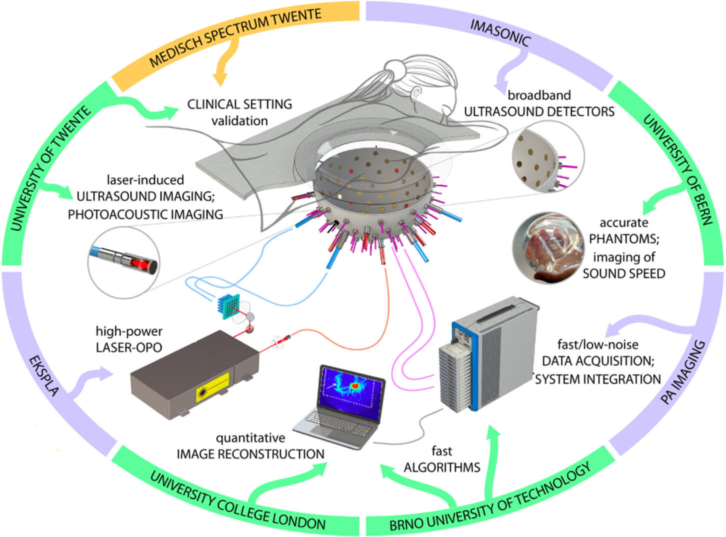

Photoacoustic Mammography Scanner

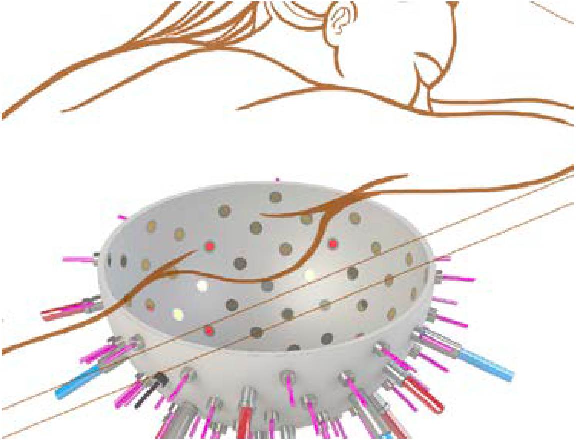

- 512 US transducers on rotatable half-sphere
- 40 optical fibers for photoacoustic excitation
- 40 inserts for laser-induced US (LIUS)

Mathematical Modelling (simplified)

Quantitative Photoacoustic Tomography (QPAT)

radiative transfer equation (RTE) + acoustic wave equation

$$(v \cdot \nabla + \mu_a(x) + \mu_s(x))\, \phi(x,v) = q(x,v) + \mu_s(x) \int \Theta(v,v')\phi(x,v')dv',$$

$$p^{PA}(x,t=0) = p_0 := \Gamma(x)\mu_a(x) \int \phi(x,v)dv, \qquad \partial_t p^{PA}(x,t=0) = 0$$

$$(c(x)^{-2}\partial_t^2 - \Delta)p^{PA}(x,t) = 0, \qquad f^{PA} = Mp^{PA}$$

Ultrasound Computed Tomography (USCT)

$$(c(x)^{-2}\partial_t^2 - \Delta)p^{US}(x,t) = s(x,t), \qquad f^{US} = Mp^{US}$$

Step-by-step inversion

1. $f^{US} \to c$: acoustic parameter identification from boundary data.
2. $f^{PA} \to p_0$: acoustic initial value problem with boundary data.
3. $p_0 \to \mu_a$: optical parameter identification from internal data.

Mathematical Modelling (simplified)

Quantitative Photoacoustic Tomography (QPAT)

radiative transfer equation (RTE) + acoustic wave equation

$$(v \cdot \nabla + \mu_a(x) + \mu_s(x))\,\phi(x,v) = q(x,v) + \mu_s(x)\int \Theta(v,v')\phi(x,v')dv',$$

$$p^{PA}(x,t=0) = p_0 := \Gamma(x)\mu_a(x)\int \phi(x,v)dv, \qquad \partial_t p^{PA}(x,t=0) = 0$$

$$(c(x)^{-2}\partial_t^2 - \Delta)p^{PA}(x,t) = 0, \qquad f^{PA} = Mp^{PA}$$

Ultrasound Computed Tomography (USCT)

$$(c(x)^{-2}\partial_t^2 - \Delta)p^{US}(x,t) = s(x,t), \qquad f^{US} = Mp^{US}$$

Step-by-step inversion

1. $f^{US} \to c$: acoustic parameter identification from boundary data.
2. $f^{PA} \to p_0$: acoustic initial value problem with boundary data.
3. $p_0 \to \mu_a$: optical parameter identification from internal data.

Ultrasound Computed Tomography

USCT Reconstruction Approaches

$$(c(x)^{-2}\partial_t^2 - \Delta)p_i(x,t) = s_i(x,t), \qquad f_i = M_i p_i, \qquad i = 1, \dots, n_{src}$$

Travel time tomography (TTT): Geometrical optics approximation.

- ✓ robust & computationally efficient
- ! valid for high frequencies ($\rightarrow$ attenuation), low res, data size

Reverse time migration (RTM): forward wavefield correlated in time with backward wavefield (adjoint wave equation) via imaging condition.

- ✓ 2 wave simulations, better quality than TTT.
- ! approximation, needs initial guess, quantitative errors

Full waveform inversion (FWI): fit full model to all data:

- ✓ high res from little data, include constraints, regularization
- ! many wave simulations, non-convex PDE-constrained optimization.

time domain vs frequency domain methods

Time Domain Full Waveform Inversion

$$F(c)p_i := (c^{-2}\partial_t^2 - \Delta)p_i = s_i, \qquad f_i = M_i\, p_i, \quad i = 1, \ldots, n_{src}$$

$$\min_{c \in \mathcal{C}} \sum_i^{n_{src}} \mathcal{D}\left(f_i(c), f_i^\delta\right) \quad s.t. \quad f_i(c) = M_i F^{-1}(c) s_i$$

$\nabla_c \mathcal{D}\left(f(c), f^\delta\right)$ for **first-order optimization** via **adjoint state method**:

$$\frac{\partial F}{\partial c} p + F \frac{\partial p}{\partial c} = 0 \quad \Rightarrow \quad \frac{\partial p}{\partial c} = -F^{-1} \frac{\partial F}{\partial c} p \quad \Rightarrow \quad \frac{\partial f}{\partial c} = -MF^{-1} \frac{\partial F}{\partial c} p$$

$$\Rightarrow \quad \frac{\partial D}{\partial c} = \left(\frac{\partial f}{\partial c}\right)^T \frac{\partial D}{\partial f} = -\left(\frac{\partial F}{\partial c} p\right)^T F^{-T} M^T \frac{\partial D}{\partial f}$$

$$\nabla_c \mathcal{D}\left(f(c), f^\delta\right) = 2 \int_0^T \frac{1}{c(x)^3} \left(\frac{\partial^2 p(x,t)}{\partial t^2}\right) q^*(x,t),$$

where $\quad (c^{-2}\partial_t^2 - \Delta) q^* = s^*, \quad s^*(x,t)$ is time-reversed data discrepancy

$\rightarrow$ **two wave simulations for one gradient**

Acoustic Wave Propagation: Numerical Solution

- **Direct methods**, such as finite-difference, pseudospectral, finite/spectral element, discontinous Galerkin.
- **Integral wave equation methods**, e.g. boundary element
- **Asymptotic methods**, e.g., geometrical optics, Gaussian beams

Acoustic Wave Propagation: Numerical Solution

- Direct methods, such as finite-difference, **pseudospectral**, finite/spectral element, discontinous Galerkin.
- Integral wave equation methods, e.g. boundary element.
- Asymptotic methods, e.g., geometrical optics, Gaussian beams.

k-Wave: *k*-space pseudospectral method solving the underlying system of first order conservation laws.

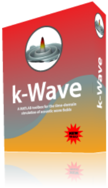

- Compute spatial derivatives in Fourier space: 3D FFTs.
- Modify finite temporal differences by *k*-space operator and use staggered grids for accuracy and robustness.
- Perfectly matched layer to simulate free-space propagation.
- Parallel/GPU computing leads to massive speed-ups.

♣ **B. Treeby and B. Cox, 2010.** k-Wave: MATLAB toolbox for the simulation and reconstruction of photoacoustic wave fields, *Journal of Biomedical Optics.*

Numerical Phantoms

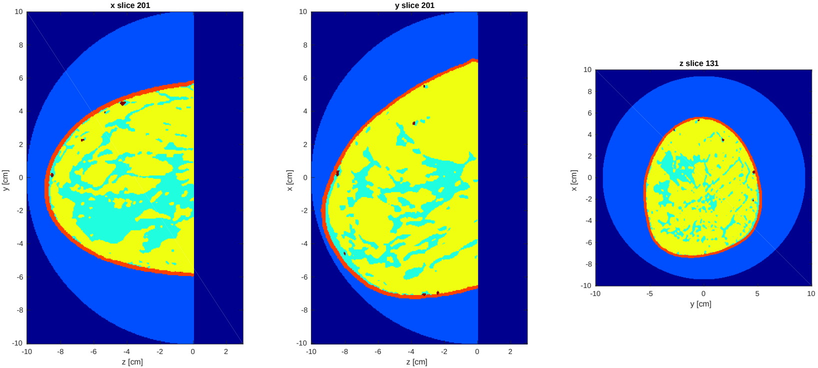

- Based on contrast enhanced MRI of prone but free-hanging breasts.
- **SOS:** background (water) 1500 m/s, fibro-glandular 1515 m/s, skin 1650 m/s, fat 1470 m/s, blood vessel 1584 m/s
- **Lou et al.** Generation of anatomically realistic numerical phantoms for photoacoustic and ultrasonic breast imaging, *JBO, 2017.*.
  https://anastasio.wustl.edu/downloadable-contents/oa-breast/

Numerical Phantoms

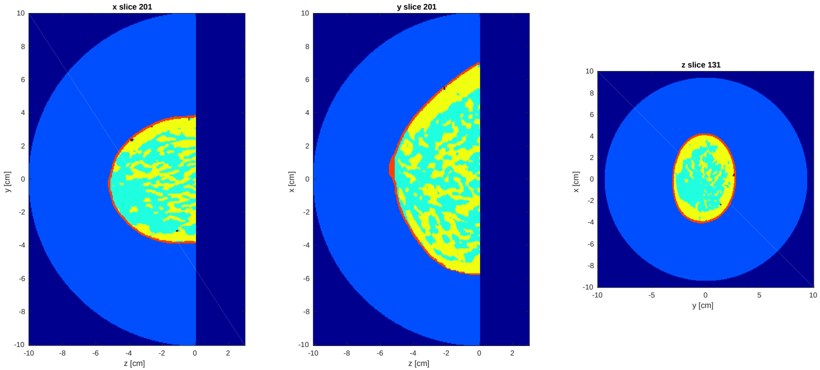

- Based on contrast enhanced MRI of prone but free-hanging breasts.
- **SOS:** background (water) 1500 m/s, fibro-glandular 1515 m/s, skin 1650 m/s, fat 1470 m/s, blood vessel 1584 m/s
- **Lou et al.** Generation of anatomically realistic numerical phantoms for photoacoustic and ultrasonic breast imaging, *JBO, 2017.*. https://anastasio.wustl.edu/downloadable-contents/oa-breast/

Numerical Phantoms (cont'd)

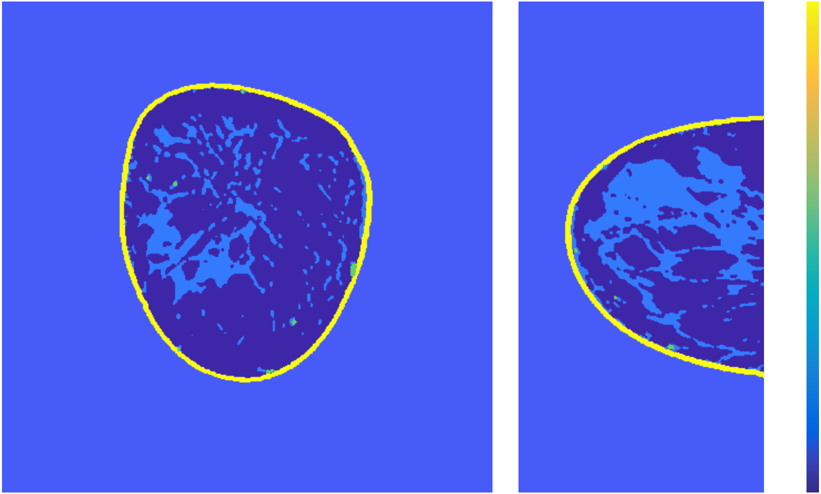

color range 1470 - 1650 m/s, resolution 0.5mm

Numerical Phantoms (cont'd)

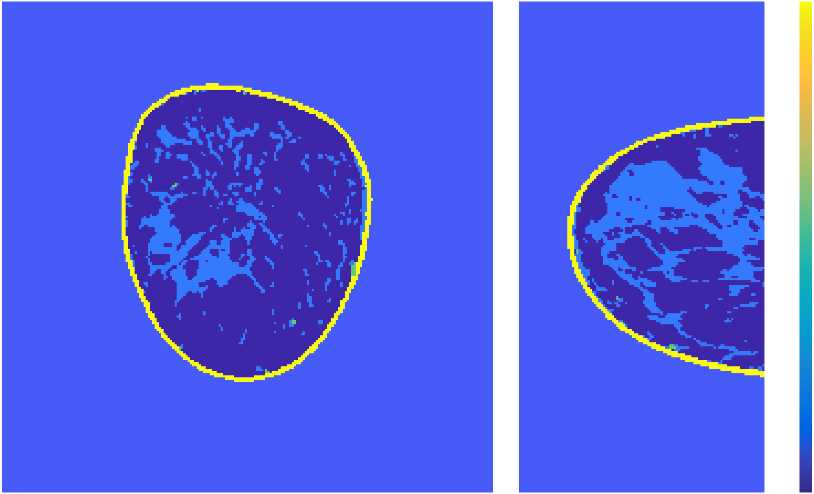

color range 1470 - 1650 m/s, resolution 1mm

Numerical Phantoms (cont'd)

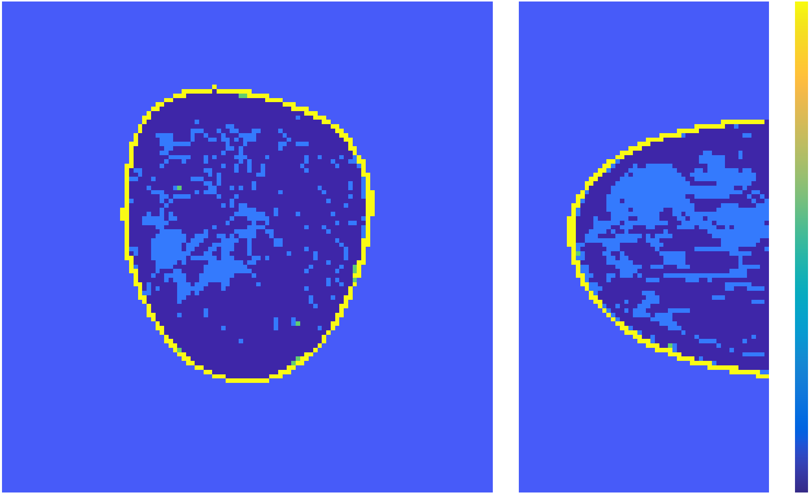

color range 1470 - 1650 m/s, resolution 2mm

FWI Illustration in 2D

SOS ground truth c^{true}

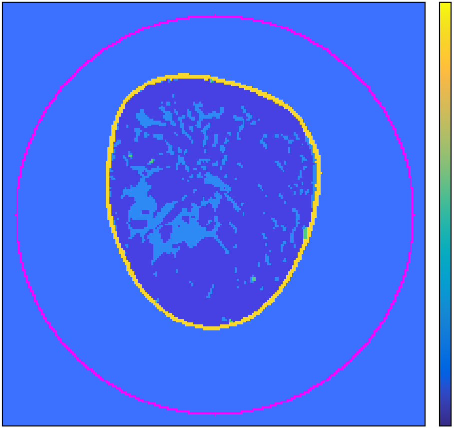

color range 1450 - 1670 m/s

- 1mm resolution
- 222^2 voxel
- 836 voxels on surface (pink)
- TTT would need 836^2 source-receiver combos for high res result

FWI Illustration in 2D: 64 Sensors, 64 Receivers

SOS reconstruction c^{rec}

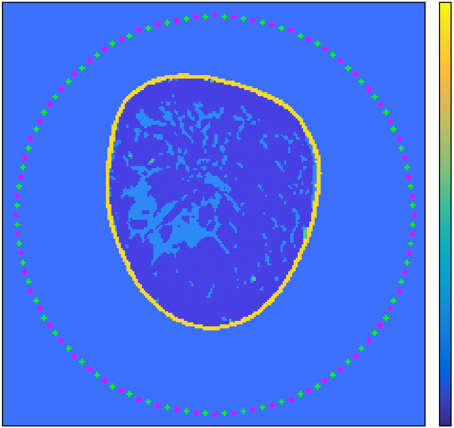

color range 1450 - 1670 m/s

reconstruction error $c^{true} - c^{rec}$

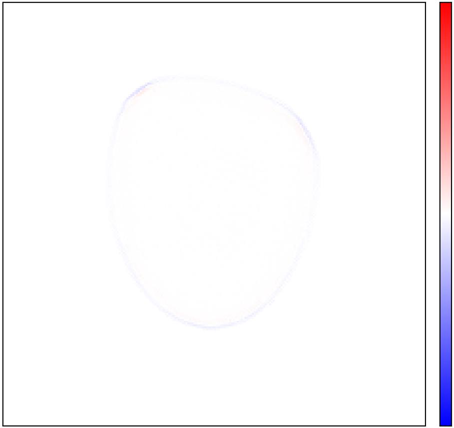

color range -50 - 50 m/s

FWI Illustration in 2D: 32 Sensors, 32 Receivers

SOS reconstruction c^{rec}

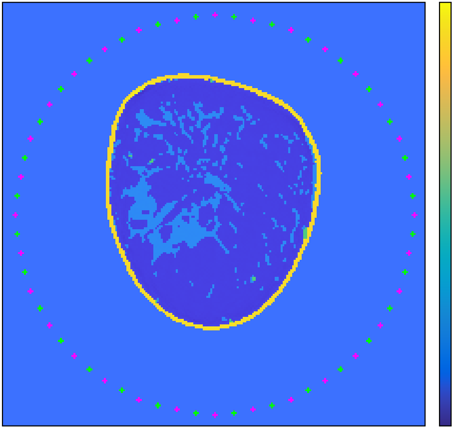

color range 1450 - 1670 m/s

reconstruction error $c^{true} - c^{rec}$

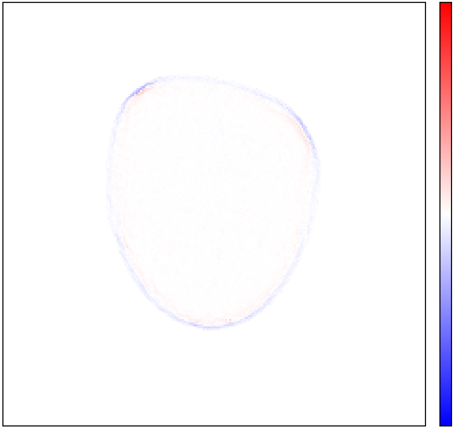

color range -50 - 50 m/s

FWI Illustration in 2D: 16 Sensors, 16 Receivers

SOS reconstruction c^{rec}

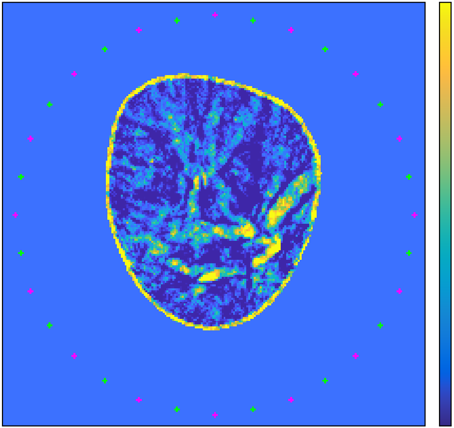

color range 1450 - 1670 m/s

reconstruction error $c^{true} - c^{rec}$

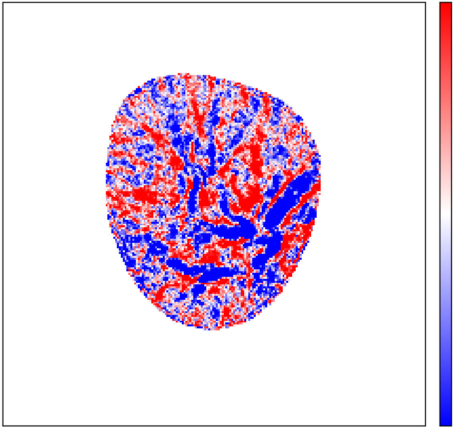

color range -50 - 50 m/s

Challenges of High-Resolution FWI in 3D

$$\min_{c \in \mathcal{C}} \sum_{i}^{n_{src}} \mathcal{D}\left(f_i(c), f_i^\delta\right) \quad s.t. \quad f_i(c) = M_i F^{-1}(c) s_i$$

$$\nabla_c \mathcal{D}\left(f(c), f^\delta\right) = 2 \int_0^T \frac{1}{c(x)^3} \left(\frac{\partial^2 p(x,t)}{\partial t^2}\right) q^*(x,t)$$

PAMMOTH scanner example:

- 0.5mm res: comp grid $560 \times 560 \times 300$ voxel $= 94$M, ROI $= 7$M
- 512 sensors, 4000 time samples (multiple simultaneous sources);

Gradient computation:

- 1 wave sim: $\sim$30 min.

! **2 wave sim per source**, $n_{src} = 512 \rightarrow 10$ days per gradient.

! **storage of forward field** in ROI: $\sim$ 200GB.

Challenges of High-Resolution FWI in 3D

$$\min_{c \in \mathcal{C}} \sum_{i}^{n_{src}} \mathcal{D}\left(f_i(c), f_i^\delta\right) \quad s.t. \quad f_i(c) = M_i F^{-1}(c) s_i$$

$$\nabla_c \mathcal{D}\left(f(c), f^\delta\right) = 2 \int_0^T \frac{1}{c(x)^3} \left(\frac{\partial^2 p(x,t)}{\partial t^2}\right) q^*(x,t)$$

PAMMOTH scanner example:

- 0.5mm res: comp grid $560 \times 560 \times 300$ voxel $= 94$M, ROI $= 7$M
- 512 sensors, 4000 time samples (multiple simultaneous sources);

Gradient computation:

- 1 wave sim: $\sim$30 min.
- ! **2 wave sim per source**, $n_{src} = 512 \rightarrow 10$ days per gradient.
  stochastic gradient methods $\rightarrow$ 90 min per gradient
- ! **storage of forward field** in ROI: $\sim$ 200GB.
  time-reversal based gradient computation $\rightarrow 5 - 25$GB.

Stochastic Gradient Optimization

$$\mathcal{J} := n_{src}^{-1} \sum_{i}^{n_{src}} \mathcal{D}_i(c) := n_{src}^{-1} \sum_{i}^{n_{src}} \mathcal{D}\left(M_i F^{-1}(c) s_i, f_i^{\delta}\right)$$

approx $\nabla\mathcal{J}$ by $|\mathcal{S}|^{-1} \sum_{j \in \mathcal{S}} \nabla\mathcal{D}_j(c)$, $\mathcal{S} \subset \{1, \ldots, n_{src}\}$ predetermined.
$\rightarrow$ **incremental gradient, ordered sub-set methods**

Stochastic Gradient Optimization

$$\mathcal{J} := n_{src}^{-1} \sum_{i}^{n_{src}} \mathcal{D}_i(c) := n_{src}^{-1} \sum_{i}^{n_{src}} \mathcal{D}\left(M_i F^{-1}(c) s_i, f_i^{\delta}\right)$$

approx $\nabla \mathcal{J}$ by $|\mathcal{S}|^{-1} \sum_{j \in \mathcal{S}} \nabla \mathcal{D}_j(c)$, $\mathcal{S} \subset \{1, \ldots, n_{src}\}$ predetermined.
$\rightarrow$ **incremental gradient, ordered sub-set methods**

Instance of **finite sum minimization** similar to training in machine learning. Use **stochastic gradient descent (SGD)**:

- momentum, gradient/iterate averaging (SAV, SAGA), variance reduction (SVRG), choice of step size, mini-batch size
- include non-smooth regularizers (SPDHG, SADMM)
- quasi-Newton-type methods,, e.g., **stochastic L-BFGS**

Bottou, Curtis, Nocedal. Optimization Methods for Large-Scale Machine Learning, *arXiv:1606.04838.*

Fabien-Ouellet, Gloaguen, Giroux, 2017. A stochastic L-BFGS approach for full-waveform inversion, *SEG.*

Gradient Estimates: Sub-Sampling vs Source Encoding

Computationally & stochastically efficient gradient estimator?

Gradient Estimates: Sub-Sampling vs Source Encoding

Computationally & stochastically efficient gradient estimator?

Source Encoding for linear PDE constraints:

$$\text{Let} \quad \hat{s} := \sum_{i}^{n_{srt}} w_i s_i, \quad \hat{f}^{\delta} := \sum_{i}^{n_{srt}} w_i f_i^{\delta}, \quad \text{with} \quad \mathbb{E}\left[w\right] = 0, \ \mathbb{C}\text{ov}[w] = I,$$

$$\text{then} \quad \mathbb{E}\left[\nabla \left\| MF^{-1}(c)\hat{s} - \hat{f}^{\delta} \right\|_2^2\right] = \nabla \sum_{i}^{n_{src}} \left\| MF^{-1}(c)s_i - f_i^{\delta} \right\|_2^2$$

- related to covariance trace estimators
- Rademacher distribution ($w_i = \pm 1$ with equal prob)
- add time-shifting for time-invariant PDEs $\rightarrow$ variance control
- can be turned into scanning strategy

Haber, Chung, Herrmann, 2012. An effective method for parameter estimation with PDE constraints with multiple right-hand sides, *SIAM J. Optim.*

Stochastic Optimization Illustration

SOS reconstruction c^{rec} L-BFGS

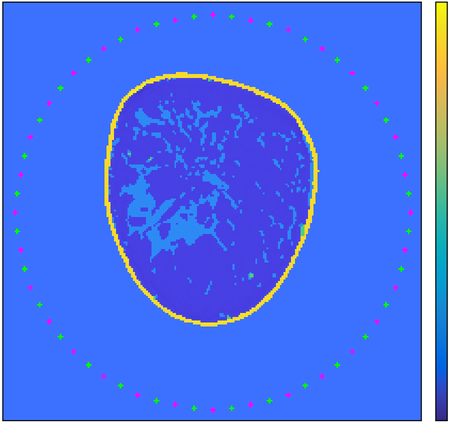

color range 1450 to 1670 m/s

reconstruction error $c^{true} - c^{rec}$

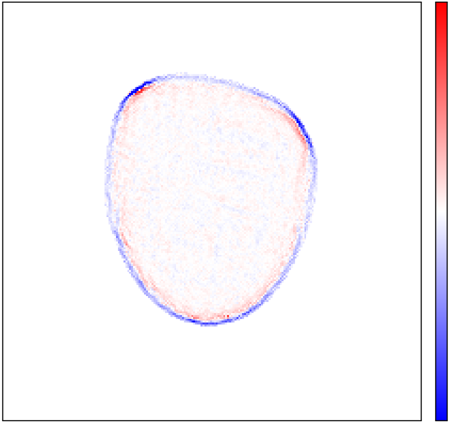

color range -10 to 10 m/s

Stochastic Optimization Illustration

SOS reconstruction c^{rec} SL-BFGS

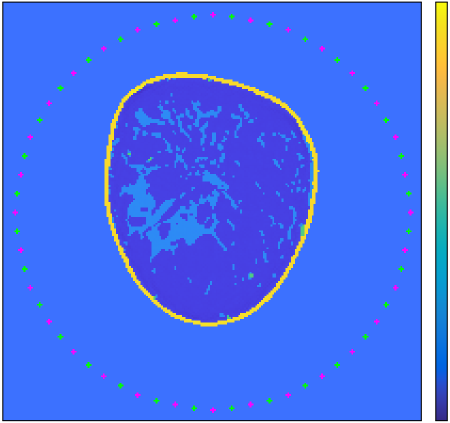

color range 1450 to 1670 m/s

reconstruction error $c^{true} - c^{rec}$

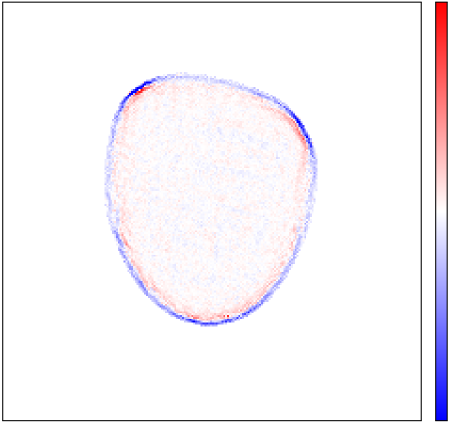

color range -10 to 10 m/s

Time-Reversal Gradient Computations

Avoid storage of forward fields!

$$(c(x)^{-2}\partial_t^2 - \Delta)p(x,t) = s(x,t), \qquad \mathit{in}\ \mathbb{R}^d \times [0, T]$$

$$\nabla_c \mathcal{D} = 2\int_0^T \frac{1}{c(x)^3}\left(\frac{\partial^2 p(x,t)}{\partial t^2}\right) q^*(x,t)$$

Idea: ROI Ω, $\mathrm{supp}(s) \in \Omega^c \times [0, T]$. As $p(x,0) = p(x,T) = \partial_t p(x,0) = \partial_t p(x,T) = 0$ in Ω, $p(x,t)$ can be reconstructed from $p(x,t)$ on $\partial\Omega \times [0, T]$ by **time-reversal (TR)**.

- store fwd fields on ROI boundary during forward wave simulation
- interleave backward (adjoint) simulation with TR of boundary data
- 3 instead of 2 wave simulations (unless 2 GPUs used).
- code up efficiently
- multi-layer boundary increases accuarcy for pseudospectral method

Putting it all together

3D breast phantom at 1mm resolution, 512 sources and sensors

true SOS

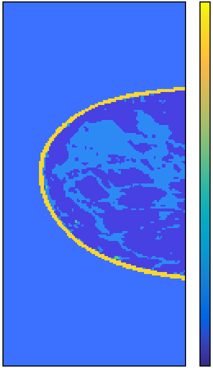

color range 1450 to 1670 m/s

sources and sensors (artificial)

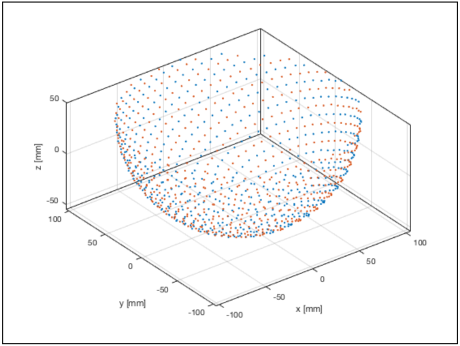

Putting it all together

3D breast phantom at 1mm resolution, 512 sources and sensors

SL-BFGS recon

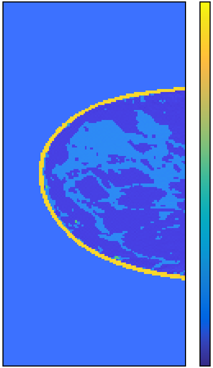

color range 1450 to 1670 m/s

reconstruction error $c^{true} - c^{rec}$

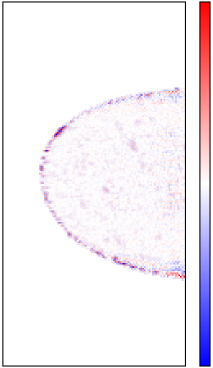

color range -15 to 15 m/s

Summary & Outlook USCT

Summary:

- proof-of-concept studies of FWI for high resolution USCT
- Stochastic L-BFGS with source encoding
- time reversal based gradient computation
- work in progress!

Outlook:

- improve initialization:
  TTT followed by multigrid (downscaling by 2: 16x speed up)
- multi-GPU CUDA code
- extension to acoustic attenuation, density, etc.
- **validation on experimental data!**

Quantitative Photoacoustic Tomography

Photoacoustic Imaging: Spectral Properties

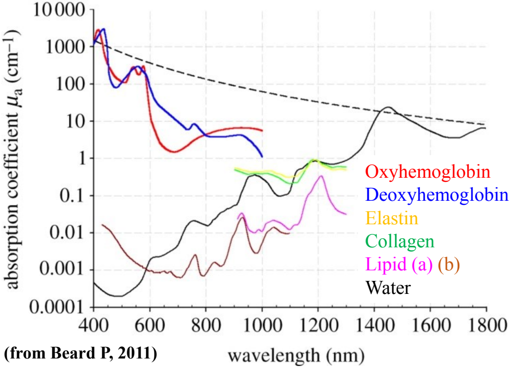

(from Beard P, 2011)

- Different wavelengths allow quantitative spectroscopic examinations.
- Gap between oxygenated and deoxygenated blood.
- Use of contrast agents for molecular imaging.

sources: Paul Beard, 2011; Jathoul et al., 2015.

Photoacoustic Imaging: Spectral Properties

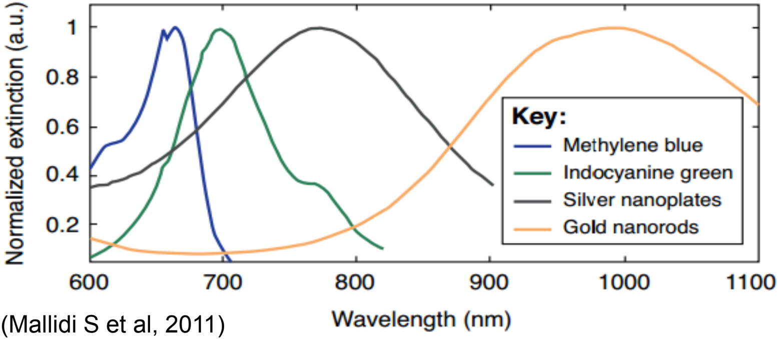

(Mallidi S et al, 2011)

- Different wavelengths allow quantitative spectroscopic examinations.
- Gap between oxygenated and deoxygenated blood.
- Use of contrast agents for molecular imaging.

sources: Paul Beard, 2011; Jathoul et al., 2015.

Quantitative Photoacoustic Tomography (QPAT)

Aim: 3D high-resolution, high sensitivity, quantitative information about physiologically relevant parameters such as chromophore concentration.

- Complete inversion (acoustic + optical + spectral).
- Model-based approaches promising.

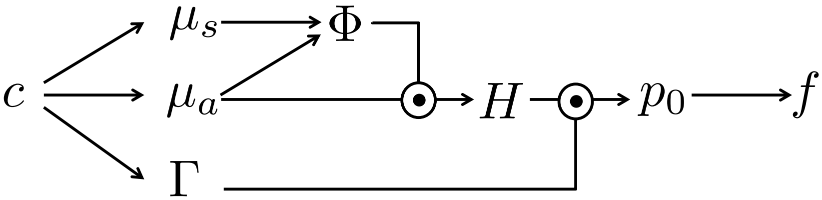

Cox, Laufer, Arridge, Beard, 2011. Quantitative spectroscopic photoacoustic imaging: a review, *Journal of Biomedical Optics.*

Quantitative Photoacoustic Tomography (QPAT)

Aim: 3D high-resolution, high sensitivity, quantitative information about physiologically relevant parameters such as chromophore concentration.

- Complete inversion (acoustic + optical + spectral).
- Model-based approaches promising.

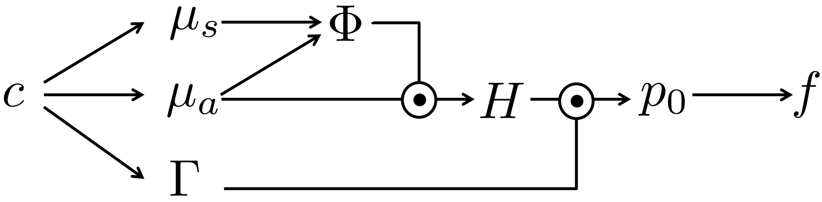

Big gap between simulations and experimental verifications!

Cox, Laufer, Arridge, Beard, 2011. Quantitative spectroscopic photoacoustic imaging: a review, *Journal of Biomedical Optics.*

QPAT Experiment: Overview

1. **Phantom development**
   - realistic, stable phantom (matching blood, in-vivo environment).
   - characterization of optical, acoustic and thermoelastic properties.
2. **Experimental measurements**
   - accurate, absolute measurements of acoustic field.
   - measurement of optical excitation parameters.
3. **Acoustic reconstruction**
   - quantitative, high-res 3D recon of initial acoustic pressure.
4. **Optical reconstruction**
   - quantitative, high-res 3D recon of chromophore concentrations.

Fonseca, Malone, L, Ellwood, An, Arridge, Beard, Cox, 2017.
Three-dimensional photoacoustic imaging and inversion for accurate quantification of chromophore distributions, *Proc. SPIE 2017.*

The Phantom

Aim: Similar properties as oxy- and deoxyhemoglobin.

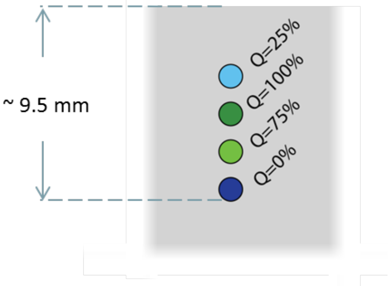

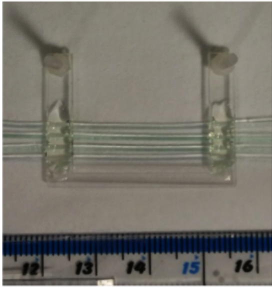

- 4 polythene tubes (580μm inner diameter, 190μm wall thickness).
- copper sulphate ($CuSO_4.5H_2O$) and nickel sulphate ($NiSO_4.6H_2O$): photostable, absorption linear with concentration.
- mixtures with Q % ratio of $NiSO_4.6H_2O$ mother solution.
- background intralipid and india ink solution as scattering medium

The Phantom

Aim: Similar properties as oxy- and deoxyhemoglobin.

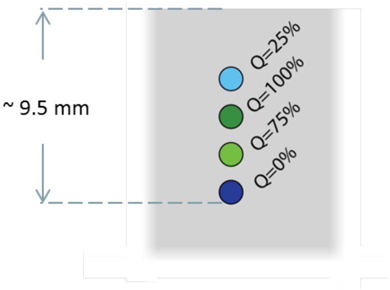

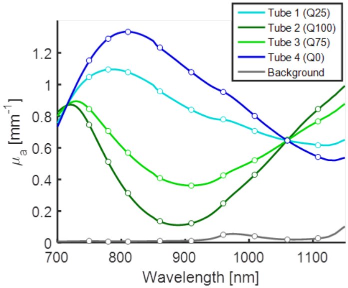

- 4 polythene tubes (580μm inner diameter, 190μm wall thickness).
- copper sulphate ($CuSO_4.5H_2O$) and nickel sulphate ($NiSO_4.6H_2O$): photostable, absorption linear with concentration.
- mixtures with Q % ratio of $NiSO_4.6H_2O$ mother solution.
- background intralipid and india ink solution as scattering medium
- spectra measured with spectrophotometer

The Phantom

Aim: Similar properties as oxy- and deoxyhemoglobin.

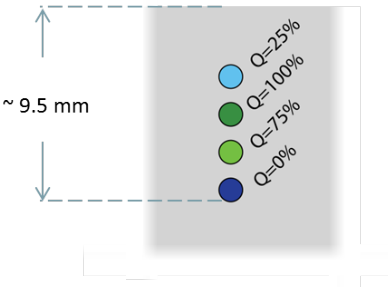

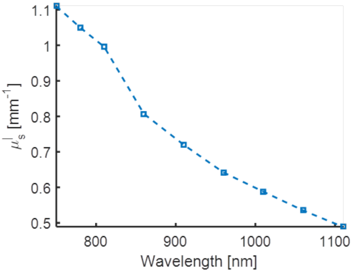

- 4 polythene tubes (580μm inner diameter, 190μm wall thickness).
- copper sulphate ($CuSO_4.5H_2O$) and nickel sulphate ($NiSO_4.6H_2O$): photostable, absorption linear with concentration.
- mixtures with Q % ratio of $NiSO_4.6H_2O$ mother solution.
- background intralipid and india ink solution as scattering medium
- spectra measured with spectrophotometer

The Phantom

Aim: Similar properties as oxy- and deoxyhemoglobin.

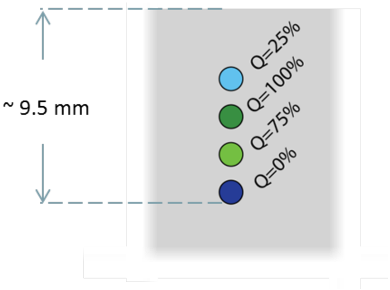

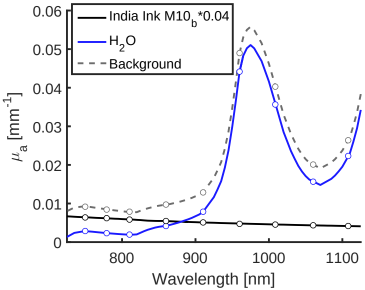

- 4 polythene tubes (580μm inner diameter, 190μm wall thickness).
- copper sulphate ($CuSO_4.5H_2O$) and nickel sulphate ($NiSO_4.6H_2O$): photostable, absorption linear with concentration.
- mixtures with Q % ratio of $NiSO_4.6H_2O$ mother solution.
- background intralipid and india ink solution as scattering medium
- spectra measured with spectrophotometer

Photoacoustic Efficiency / Grüneisenparameter

- $p_0 = \Gamma(c)H$
- Linear dependence found by photoacoustic spectroscopy:

$$\Gamma = \Gamma_{H_2O}\,(1 + \beta_{CuSO_4}\,c_{CuSO_4} + \beta_{NiSO_4}\,c_{NiSO_4}) \qquad \text{(range: } 1 - 1.72\text{)}$$

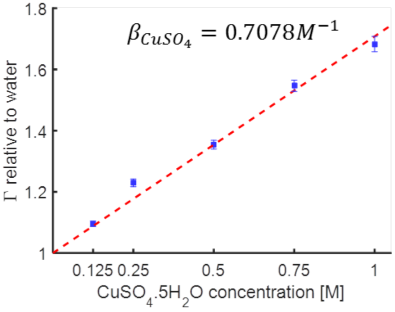

Stahl, Allen, Beard, 2014. Characterization of the thermalisation efficiency and photostability of photoacoustic contrast agents, *Proc. SPIE.*

High Resolution PAT Scanner

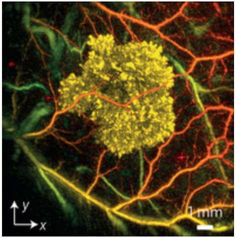

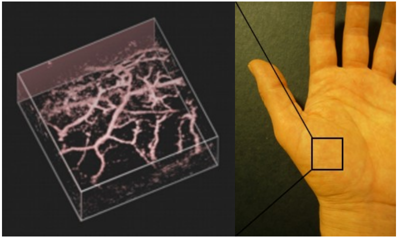

- Fabry-Pérot sensors: wide bandwidth, small element size, low noise, almost omni-directional
- data acquisition gets faster and faster

Ellwood, Ogunlade, Zhang, Beard, Cox, 2017. Photoacoustic tomography using orthogonal Fabry Pérot sensors, *Journal of Biomedical Optics*.

sources: Paul Beard, 2011; Jathoul et al., 2015, Ellwood et al., 2017.

High Resolution PAT Scanner

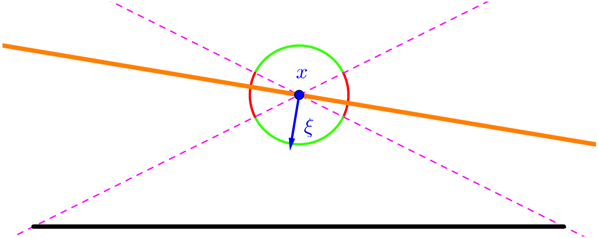

- Fabry-Pérot sensors: wide bandwidth, small element size, low noise, almost omni-directional
- data acquisition gets faster and faster

Ellwood, Ogunlade, Zhang, Beard, Cox, 2017. Photoacoustic tomography using orthogonal Fabry Pérot sensors, *Journal of Biomedical Optics.*

sources: Paul Beard, 2011; Jathoul et al., 2015, Ellwood et al., 2017.

High Resolution PAT Scanner

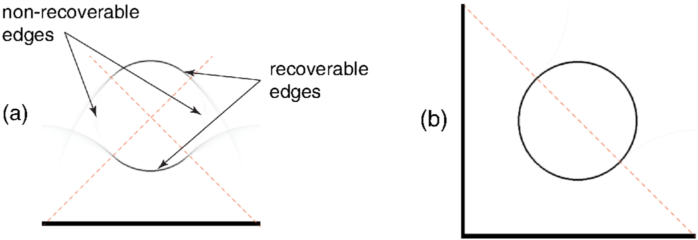

- Fabry-Pérot sensors: wide bandwidth, small element size, low noise, almost omni-directional
- data acquisition gets faster and faster
- two orthogonal sensors to reduce limited view artefacts

Ellwood, Ogunlade, Zhang, Beard, Cox, 2017. Photoacoustic tomography using orthogonal Fabry Pérot sensors, *Journal of Biomedical Optics.*

sources: Paul Beard, 2011; Jathoul et al., 2015, Ellwood et al., 2017.

High Resolution PAT Scanner

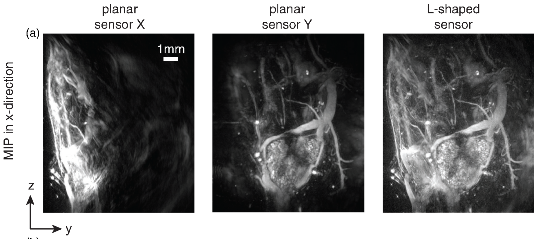

- Fabry-Pérot sensors: wide bandwidth, small element size, low noise, almost omni-directional
- data acquisition gets faster and faster
- two orthogonal sensors to reduce limited view artefacts

Ellwood, Ogunlade, Zhang, Beard, Cox, 2017. Photoacoustic tomography using orthogonal Fabry Pérot sensors, *Journal of Biomedical Optics.*

sources: Paul Beard, 2011; Jathoul et al., 2015, Ellwood et al., 2017.

Experimental Setup

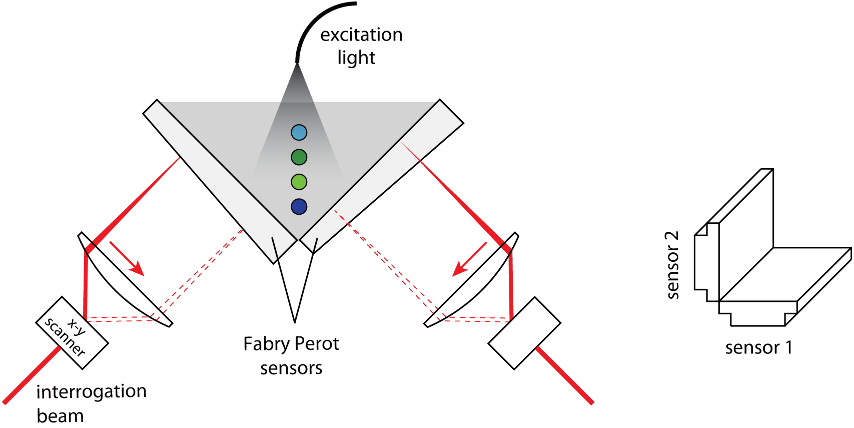

- excitation: 7ns pules at 10Hz with 19mJ at 800nm
- spatial sampling 100μm, temporal sampling: 8ns

Experimental Setup

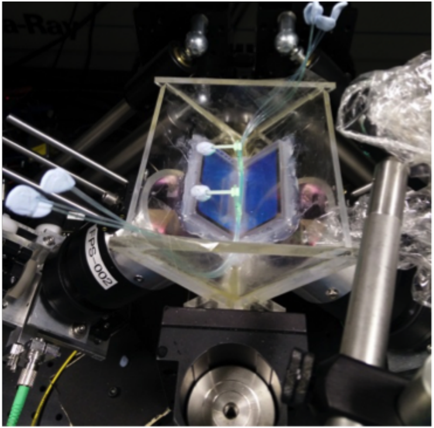

- excitation: 7ns pules at 10Hz with 19mJ at 800nm
- spatial sampling 100μm, temporal sampling: 8ns

Scanner Calibration

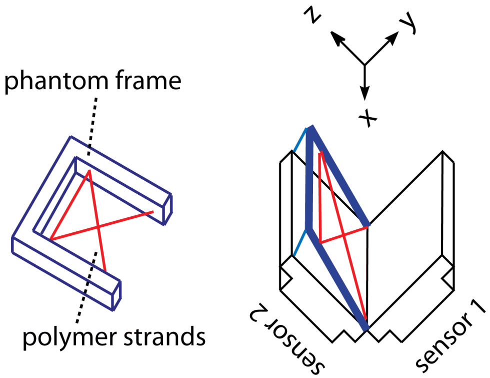

- spatial alignment with registration phantom
- V to Pa conversion by characterisation with calibrated transducer
- Pa corrected for pulse energy variations with integrating sphere

Acoustic Reconstruction

$$(c(x)^{-2}\partial_t^2 - \Delta)p^{PA}(x,t) = 0, \qquad f^{PA} = Mp^{PA}$$

$$p^{PA}(x,t=0) = p_0 := \Gamma(x)\mu_a(x)\int \phi(x,v)dv, \qquad \partial_t p^{PA}(x,t=0) = 0$$

$$f^{PA} = Ap_0$$

- pre-processing & sound speed calibration
- **model-based inversion**: $\hat{p} = \text{argmin}\ \frac{1}{2}\left\|Ap_0 - f^{PA}\right\|_2^2 \ \ s.t.\ \ p_0 \geqslant 0$ via projected gradient-descent-type scheme (iterative time reversal):

$$p^{k+1} = \Pi_+\left(p_0^k - A^{\triangleleft}(Ap_0^k - f^{PA})\right)$$

- numerical wave propagation by k-Wave.
- 50μm voxel resolution: $N = 264 \times 358 \times 360$ (up to 400^3!)

Arridge, Betcke, Cox, L, Treeby, 2016. On the Adjoint Operator in Photoacoustic Tomography, *Inverse Problems 32(11).*

Acoustic Inversion Results

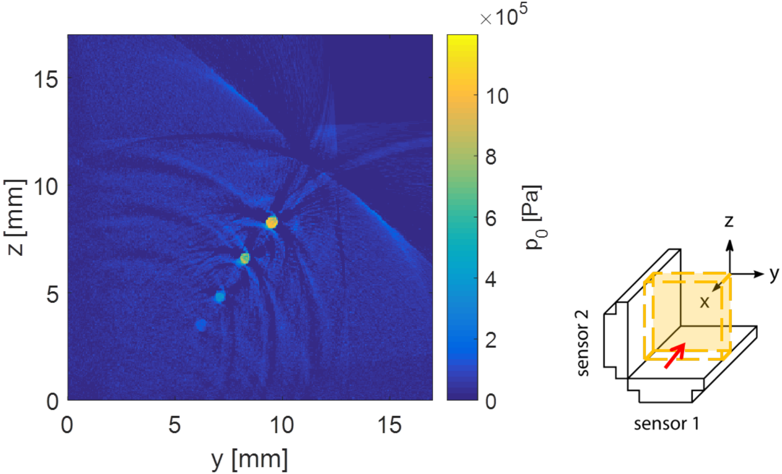

Maximum intensity projection for 1060nm excitation.

Acoustic Inversion Results

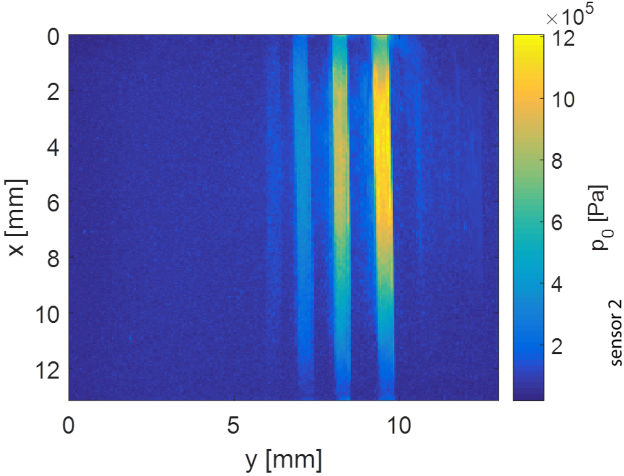

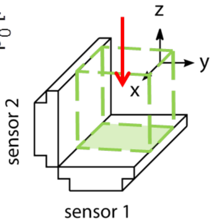

Maximum intensity projection for 1060nm excitation.

Acoustic Inversion Results

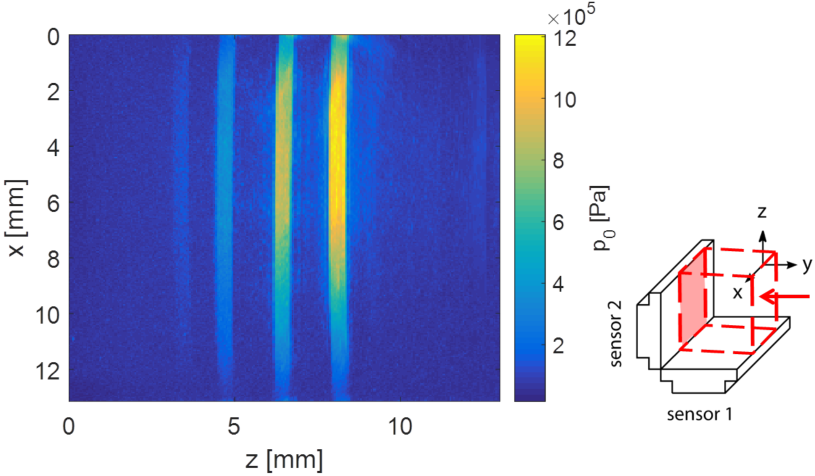

Maximum intensity projection for 1060nm excitation.

Acoustic Inversion Results

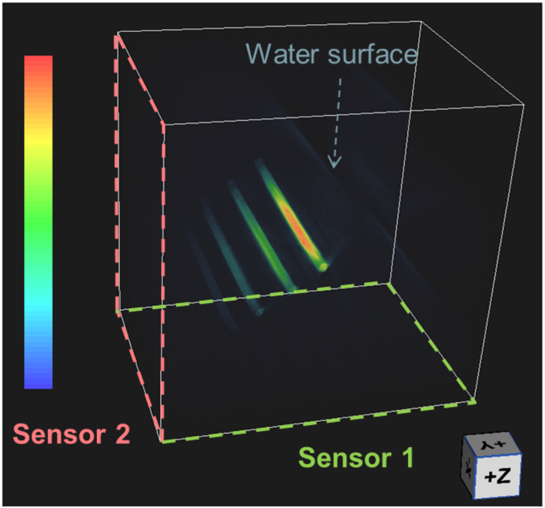

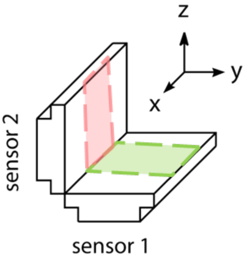

volume rendering for 1060nm excitation.

Acoustic Inversion Results: Different Inversion Approaches

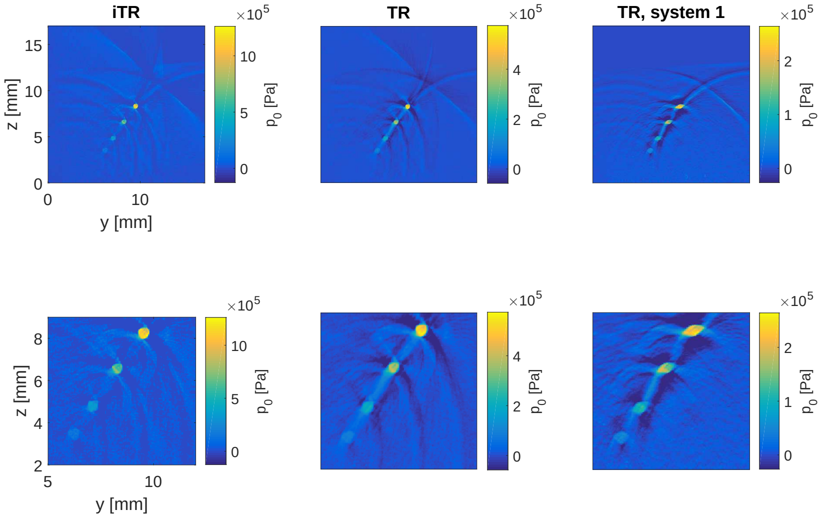

Acoustic Inversion Results: Simulation vs Experiment

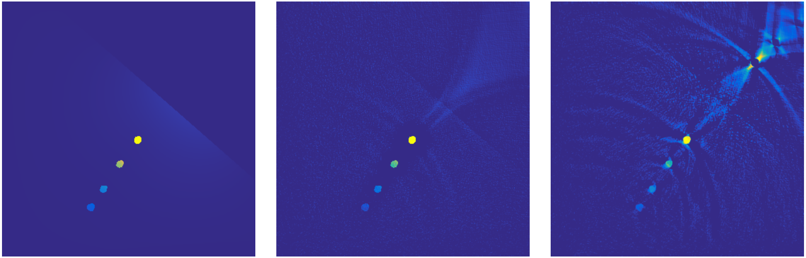

true solution | simulated data recon | experimental data recon

Optical Inversion: Overview

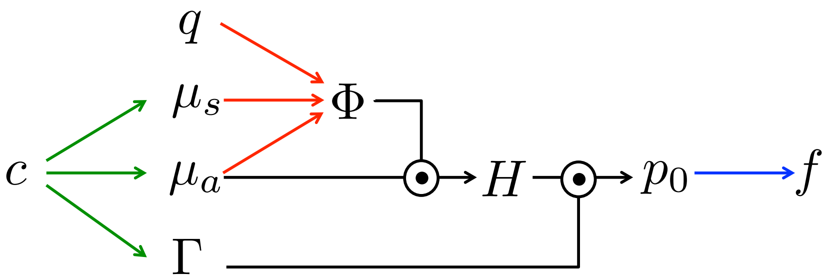

- mapping from c to (μ_a, μ_s, Γ): measured spectra
- q: light source properties
- mapping from (μ_a, μ_s, q) to Φ: **non-linear**.

Optical Reconstruction: Beam Characterization

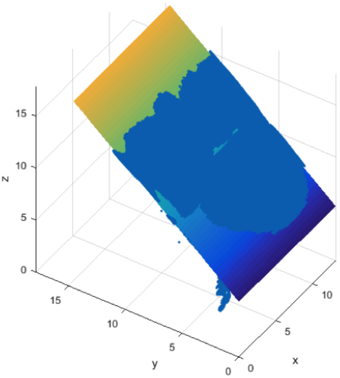

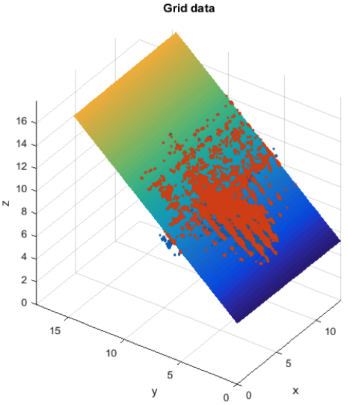

- PA image at water absorption peak to determine surface
- PA image with acetate sheet to determine center and radius

Optical Reconstruction: Beam Characterization

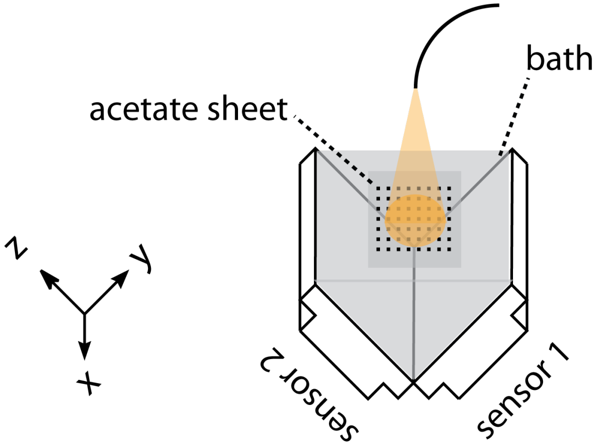

- PA image at water absorption peak to determine surface
- PA image with acetate sheet to determine center and radius

The RTE and Toast++

Radiative transfer equation

$$(v \cdot \nabla + \mu_a(x) + \mu_s(x))\,\phi(x,v) = q(x,v) + \mu_s(x)\int \Theta(v,v')\phi(x,v')dv'$$

$$\Phi(x) = \int \phi(x,v)dv,$$

! $(x,v) \in \mathbb{R}^5 \rightsquigarrow$ direct FEM infeasible.

Diffusion approximation

$$(\mu_a(x) - \nabla \cdot \kappa(x)\nabla)\,\Phi(x) = \int q(x,v)dv, \quad \kappa = \frac{1}{3(\mu_a + \mu_s(1-g))}$$

source moved one scattering wave-length into volume.

Toast++

- time-resolved light transport in highly scattering media
- FEM, different elements and basis functions, 2D and 3D

Schweiger, Arridge, 2014. The Toast++ software suite for forward and inverse modeling in optical tomography, *Journal of Biomedical Optics.*

Model Based Inversion

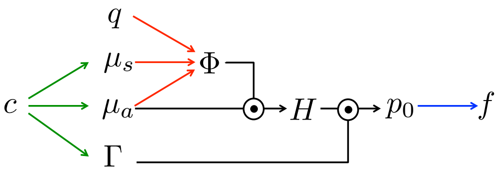

$$\hat{c} = \underset{c \in \mathcal{C}}{\operatorname{argmin}} \sum_{\lambda=1}^{N_\lambda} \int_{ROI} \left(p_{0,\lambda}^{recon} - p_{0,\lambda}(c)\right)^2 dx$$

- solve via iterative first order method (L-BFGS)
- derivatives of $\Phi(\mu_a, \mu_s)$ via adjoint method: two solves of light model per iteration (per wavelength).
- additional data interpolation and rotation into FEM mesh
- addition of global scaling factor.

Malone, Powell, Cox, Arridge, 2015. Reconstruction-classification method for quantitative photoacoustic tomography, *JBO.*

Optical Inversion Results

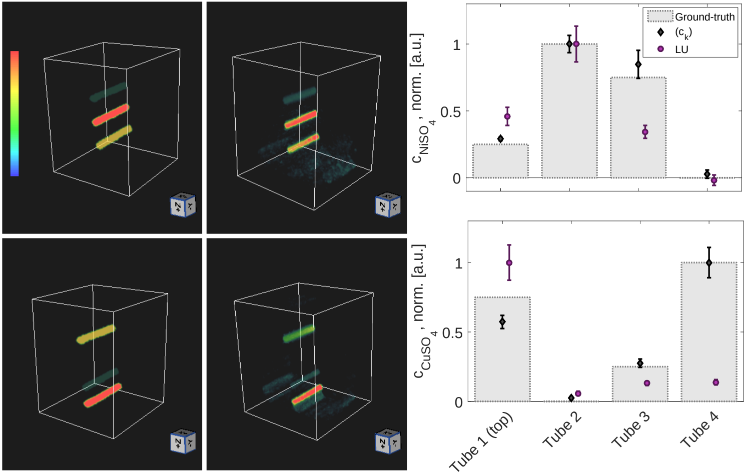

(a) (b)

Optical Inversion Results

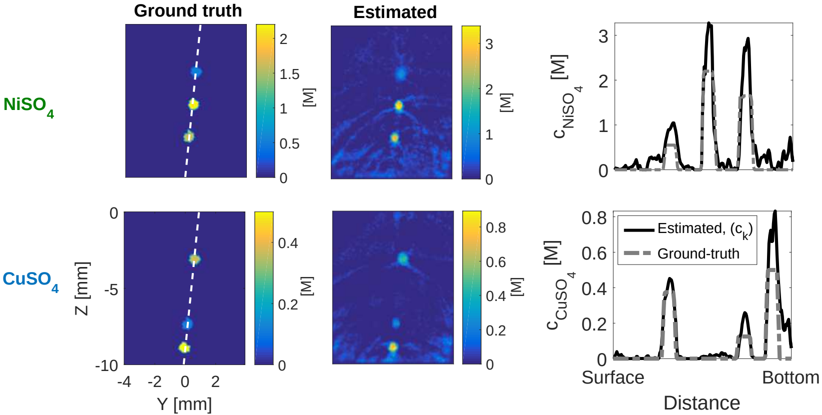

Optical Inversion Results

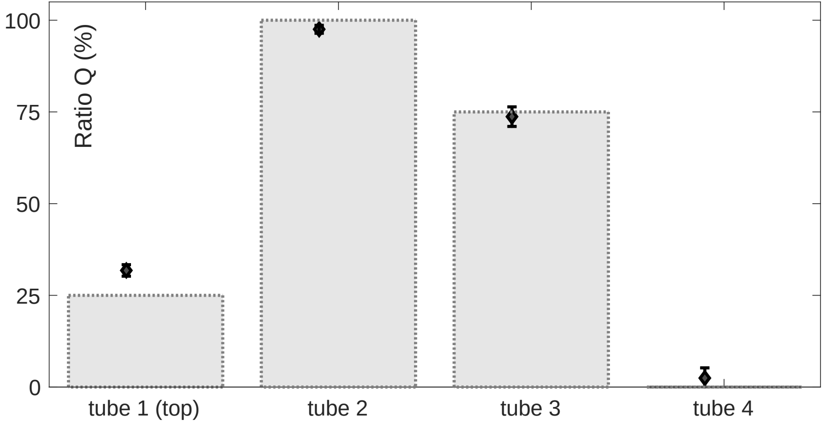

Results for ratio Q, the **sO_2 analogue**.

Effect of Inaccuracies

$$\delta_{NiSO4} = \frac{\left\| c_{true}^{(norm)} - c_{est}^{(norm)} \right\|}{\left\| c_{true}^{(norm)} \right\|}$$

Source of explicit uncertainty/error	δ_{NiSO4}
None	6.5%
μ_s: 20% overestimation	7.4%
Grüneisen: $\Gamma = \Gamma_{H_2O}$	39.6%
No acoustic pressure calibration	14.4 %
non-iterative time reversal	26.5%
non-iterative time reversal + sensor 1 only	50.7 %

Summary & Outlook QPAT

What we wanted to do:

- highly-res, 3D chromophore distributions from exp. PAT data.
- ratio between two chromophores (sO_2 analogue)

What we learned and achieved:

- promising estimates of normalized chromophore concentrations.
- promising ratio estimates
- sensitivity to in-accuracies

What we need to improve:

- experimental set-up & beam characterization
- acoustic reconstruction
- light model
- coupling of acoustic and optical models
- optimization

- **L, Pérez-Liva, Treeby, Cox, 2019.** Time-Domain Full Waveform Inversion for High Resolution 3D Ultrasound Computed Tomography of the Breast, *in preparation.*
- **Fonseca, Malone, L, Ellwood, An, Arridge, Beard, Cox, 2017.** Three-dimensional photoacoustic imaging and inversion for accurate quantification of chromophore distributions, *Proc. SPIE 2017.*

We gratefully acknowledge the support of NVIDIA Corporation with the donation of the Tesla K40 GPU used for this research.

Thank you for your attention!

- **L, Pérez-Liva, Treeby, Cox, 2019.** Time-Domain Full Waveform Inversion for High Resolution 3D Ultrasound Computed Tomography of the Breast, *in preparation.*
- **Fonseca, Malone, L, Ellwood, An, Arridge, Beard, Cox, 2017.** Three-dimensional photoacoustic imaging and inversion for accurate quantification of chromophore distributions, *Proc. SPIE 2017.*

We gratefully acknowledge the support of NVIDIA Corporation with the donation of the Tesla K40 GPU used for this research.